Engineering Transactions, **68**(1): 69–87, 2020, doi: 10.24423/EngTrans.1062.20200102
Polish Academy of Sciences • Institute of Fundamental Technological Research (IPPT PAN)
Université de Lorraine • Poznan University of Technology

Research Paper

Spectral Quasilinearization Method for Solution of Convective Heating Condition

Wubshet IBRAHIM

Department of Mathematics
Ambo University
P.O. Box 19, Ambo, Oromia 00251, Ethiopia
e-mail: wubshetib@yahoo.com

This article aims to implement the spectral quasilinearization method to examine the impact of a second-order slip flow and convective heating on boundary layer flow and heat transfer of a nanofluid over an extensible surface. The mathematical modeling of the flow problem is obtained by taking into consideration the weight of leading parameters. Similarity conversions are employed in converting the leading partial differential equations to non-linear high-order ordinary differential equations. These equations were numerically computed using a spectral quasilinearization method for different values of the main parameters. The interesting numerical outcomes are attained for the flow variables, as well as the skin friction coefficient, local Nusselt number and Sherwood number. The results designate that the skin friction coefficient C_f falls as the values of slip parameter γ rise, it improves as the values of δ boost. Both the local Nusselt number, $\theta'(0)$, and Sherwood number, $\phi'(0)$, drop as both Brownian motion and thermophoresis parameters increase. A comparison of the spectral quasilinerization method (SQLM) with the bvp4c method is conducted and an excellent agreement in their output is observed.

Key words: second-order slip flow; spectral quasilinearization method; nanofluid; heat transfer; convective heating.

Notations

B_0 – magnetic field strength,
B_i – convective parameter,
C_f – local skin friction coefficient,
c_w – concentration at the surface of the sheet,
c_∞ – ambient concentration,
D_B – Brownian diffusion coefficient,
D_T – thermophoresis diffusion coefficient,
f – dimensionless stream function,
h – dimensionless concentration function,
k – thermal conductivity,

Kn – Knudsen number,
Le – Lewis number,
M – magnetic parameter,
N_b – Brownian motion parameter,
N_t – thermophoresis parameter,
Nu_x – local Nusselt number,
Pr – Prandtl number,
Re_x – local Reynolds number,
T – temperature of the fluid inside the boundary layer,
Sh_x – local Sherwood number,
T_w – temperature at the surface of the sheet,
T_∞ – ambient temperature,
U_∞ – free stream velocity,
u, v – velocity component along x- and y-direction.

Greek
α – thermal diffusivity,
γ – first order slip condition,
δ – second order slip condition,
η – dimensionless similarity variable,
θ – dimensionless temperature,
μ – dynamic viscosity of the fluid,
υ – kinematic viscosity of the fluid,
$(\rho)_f$ – density of the basefluid,
$(\rho c)_f$ – heat capacity of the base fluid,
$(\rho c)_p$ – effective heat capacity of a nanoparticle,
σ – electrical conductivity,
τ – parameter defined by $\frac{(\rho c)_p}{(\rho c)_f}$,
ψ – stream function.

Subscripts
∞ – condition at the free stream,
w – condition at the surface.

1. Introduction

Nowadays, finding the solution of fluid flow problems via numerical method becomes a big research field due to its importance in different areas of applied sciences and engineering. Fluid flow problems are usually expressed in terms of the partial differential equation, which is a boundary value problems. Getting the solution of boundary value problems is often very difficult. There are different numerical methods of finding the solution of boundary value problems. The spectral method is one of the numerical approaches used for obtaining the solution of the non-linear system of boundary value problems. Trefethen [1] has applied the spectral method for the solutions of nonlinear differential equations.

Spectral methods have different variants such as spectral relaxation method, spectral quasilinearization method and others. For the last five years, researches have employed the numerical method called spectral quasilinearization method to find the numerical solution of fluid dynamics problems, and they have obtained excellent results with high accuracy. The mathematical representation of this method is easily straightforward and can be programmed in computer software like Matlab, Mathematica, and Maple. The method is very efficient and converges with a small number of iterations. The pioneering paper on the spectral method was presented by Shateyi and Makinde [2] on getting the solution of the problem of a radially stretching disc with convective heating. Majeet *et al.* [3] have obtained a numerical solution for non-Newtonian fluid flow and heat transfer problem over a stretching cylinder with the help of spectral quasilinearization method. Other researchers such as Motsa *et al.* [4] have used both spectral quasilinearization method and spectral relaxation for computing unsteady boundary layer flow problems. Other fluid flow problem solutions were obtained by spectral quasilinearization and spectral relaxation methods by Mosta and other authors [5–8].

The effects of second-order slip flow phenomena widely occur in fluid flow. For the last decade, researchers have investigated second-order slip flow in fluid dynamics but still there are many problems involving second-order slip flow that should be examined. Therefore, this study discusses the second-order slip flow numerically. Previously [9, 10], analytically studied the viscous flow over a shrinking sheet with a second-order slip flow model. Following them, Nandeppanavar *et al.* [11] computed the effect of second-order slip flow and heat transfer over a stretching sheet with non-linear Navier boundary condition. It has been indicated that both the first- and the second-order slip parameter, and the mass suction parameter significantly affect the flow condition and shear stress at the wall. Furthermore, Rosca and Pop [12] also examined the influences of the second-order slip flow on heat transfer over a vertical permeable stretching/shrinking sheet. The result implied that the flow and heat transfer characteristics on a stretching/shrinking sheet were strongly influenced by the parameter. Moreover, Rosca and Pop [13] investigated mixed convection stagnation point flow past a vertical flat plate with a second-order slip flow condition. Considering the magnetic field, Turkyilmazoglu [14] also obtained the analytical solution of the heat and mass transfer problem under the influence of a second-order slip flow. Singh and Chamkha [15] also discussed the dual solution for viscous fluid flow and heat transfer with a second-order slip for the shrinking sheet. More research on the spectral method is given in [16–18].

All the previous studies examined the flow problems with the second-order slip flow towards the stretching sheet with the exclusion of nanoparticles. But, nowadays, nanofluids play a great role in different heavy industry fields. There-

fore, this study targets to fill this knowledge gap in the application of the second-order slip flow.

The main goal of this paper is to analyze the combined effect of the first, second-order slip flows, magnetic and convective heating parameters on the boundary layer flow towards the stretching sheet in a nanofluid. Moreover, the effect of Brownian motion, thermophoresis parameters and nanoparticle fraction on the boundary layer flow and heat transfer due to nanofluid are examined. The governing boundary layer equations were transformed into a two-point boundary value problem using similarity variables and numerically solved using the spectral quasilinearization methods with a code programmed in Matlab. The effects of governing parameters on fluid velocity, temperature and particle concentration were discussed and shown in graphs and tables as well.

2. Mathematical formulation

This investigation deals with a solution of a steady 2D viscous flow of a nanofluid over a stretching sheet with the effects of second-order slip boundary condition. The study assumed that the surface of a sheet is heated from the bottom by convection from a hot fluid beneath the surface at temperature T_f that injects a heat transfer coefficient h_f. The boundary conditions at the sheet surface and far into the cold fluid may be written as $-k\frac{\partial T}{\partial y} = h_f(T_f - T_w)$. The uniform ambient temperature and concentration, respectively, are T_∞ and C_∞. The slip velocity condition at the surface u_{slip} is taken into account. A constant transverse magnetic field of strength $B = B_0$ is applied in the positive y-direction, perpendicular to the surface. Due to the small magnetic Reynolds number, the generated magnetic field is negligible so it is ignored. T_w, T_∞, C_w, C_∞, and B_0 are the temperature at the surface of the sheet, ambient temperature of the fluid, the concentration at the surface of the sheet, ambient concentration and magnetic field strength, respectively. The coordinate system is selected as x-axis along the extensible surface and y-axis perpendicular to it, as shown in Fig. 1.

Using the above assumptions and after boundary layer approximations, the flow equations are as described by [19]:

$$\frac{\partial u}{\partial x} + \frac{\partial v}{\partial y} = 0, \tag{2.1}$$

$$u\frac{\partial u}{\partial x} + v\frac{\partial u}{\partial y} = \upsilon\left(\frac{\partial^2 u}{\partial y^2}\right) - \frac{\sigma B_0^2}{\rho_f}(u), \tag{2.2}$$

$$u\frac{\partial T}{\partial x} + v\frac{\partial T}{\partial y} = \frac{k}{(\rho c)_p}\left(\frac{\partial^2 T}{\partial y^2}\right) + \tau\left\{D_B\left(\frac{\partial C}{\partial y}\frac{\partial T}{\partial y}\right) + \frac{D_T}{T_\infty}\left[\left(\frac{\partial T}{\partial y}\right)^2\right]\right\}, \tag{2.3}$$

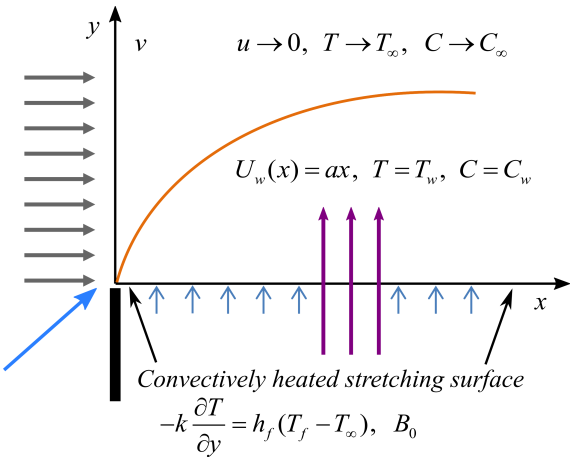

FIG. 1. Flow diagram.

$$u\frac{\partial C}{\partial x} + v\frac{\partial C}{\partial y} = D_B\left(\frac{\partial^2 C}{\partial y^2}\right) + \frac{D_T}{T_\infty}\left(\frac{\partial^2 T}{\partial y^2}\right). \tag{2.4}$$

The boundary conditions are

$$\begin{aligned} &u = u_w + U_{\text{slip}}, \qquad v = 0, \\ &-k\frac{\partial T}{\partial y} = h_f(T_f - T_\infty), \qquad C = C_w \quad \text{at} \quad y = 0, \\ &u \to U_\infty = 0, \qquad v = 0, \\ &T \to T_\infty, \qquad C = C_\infty \quad \text{as} \quad y \to \infty. \end{aligned} \tag{2.5}$$

U_{slip} is the slip velocity at the surface; slip velocity equation [20] (valid for arbitrary Knudsen number, Kn), used by researchers such as [9–11], is given by

$$\begin{aligned} U_{\text{slip}} &= \frac{2}{3}\left(\frac{3-\alpha l^2}{\alpha} - \frac{3}{2}\frac{1-l^2}{\text{Kn}}\right)\lambda\frac{\partial u}{\partial y} - \frac{1}{4}\left[l^4 + \frac{2}{\text{Kn}^2}(1-l^2)\right]\lambda^2\frac{\partial^2 u}{\partial y^2}, \\ U_{\text{slip}} &= A\frac{\partial u}{\partial y} + B\frac{\partial^2 u}{\partial y^2}, \end{aligned} \tag{2.6}$$

where A and B are constant, Kn is Knudsen number, $l = \min\left[\frac{1}{\text{Kn}}, 1\right]$, α is the momentum accommodation coefficient with $0 \le \alpha \le 1$, and λ is the molecular mean free path. Based on the definition of l, it is noticed that for any given value of Kn, we have $0 \le l \le 1$. The molecular mean free path is always positive. Thus we know that $B < 0$, and hence the second term on the right-hand side

of Eq. (2.6) is a positive number. Moreover, γ is the first-order velocity slip parameter with $\gamma = A\sqrt{\frac{a}{\nu}}$, which is positive, δ is the second-order velocity slip parameter with $\delta = \frac{Ba}{\nu}$ being negative. The velocity components along x- and y-axis are u and v, respectively. υ is the kinematic viscosity, T is the temperature inside the boundary layer, $(\rho c)_p$ is the effective heat capacity of a nanoparticle, ρ is the density, T_∞ is the ambient temperature far away from the sheet.

The following are the dimensionless quantities used during the transformation:

$$\eta = \sqrt{\frac{a}{\upsilon}}y, \quad \psi = \sqrt{a\upsilon}xf(\eta), \quad \theta(\eta) = \frac{T - T_\infty}{T_f - T_\infty}, \quad \phi(\eta) = \frac{C - C_\infty}{C_w - C_\infty}. \tag{2.7}$$

The equation of continuity is satisfied if we choose a stream function $\psi(x, y)$ such that

$$u = \frac{\partial \psi}{\partial y}, \qquad v = -\frac{\partial \psi}{\partial x}. \tag{2.8}$$

By applying the similarity transformation variables, the leading Eqs (2.1)–(2.4) are converted to the high-order ordinary differential equation as follows:

$$f''' + ff'' - f'^2 - Mf' = 0, \tag{2.9}$$

$$\theta'' + \Pr\left[f\theta' + N_b\phi'\theta' + N_t\theta'^2\right] = 0, \tag{2.10}$$

$$\phi'' + \mathrm{Le}\,\Pr f\phi' + \frac{N_t}{N_b}\theta'' = 0, \tag{2.11}$$

with boundary conditions

$$\begin{aligned} &f(0) = 0, \qquad f'(0) = 1 + \gamma f''(0) + \delta f'''(0), \\ &\theta'(0) = -B_i(1 - \theta(0)), \qquad \phi(0) = 1, \quad \text{at} \quad \eta = 0, \\ &f'(\infty) \to 0, \qquad \theta(\infty) \to 0, \qquad \phi(\infty) \to 0, \quad \text{as} \quad \eta \to \infty, \end{aligned} \tag{2.12}$$

where the influencing parameters are defined by:

$$\left.\begin{aligned} &\Pr = \frac{\upsilon}{\alpha}, \qquad B_i = \frac{h_f}{k_f}\sqrt{\frac{\upsilon}{a}} \\ &M = \frac{\sigma B_0^2}{\rho_f a}, \qquad \mathrm{Le} = \frac{\upsilon}{D_B} \\ &N_b = \frac{(\rho c)_p D_B(C_w - C_\infty)}{(\rho c)_f \upsilon} \\ &N_t = \frac{(\rho c)_p D_T(T_w - T_\infty)}{(\rho c)_f \upsilon T_\infty} \end{aligned}\right\} \text{Governing parameters,} \tag{2.13}$$

where f', θ and ϕ are the flow field velocity, temperature and particle concentration, respectively, η is the similarity variable, the prime denotes differentiation with respect to η. γ, δ, Pr, M, N_b, N_t, Le denote first-order slip parameter, second-order slip parameter, Prandtl number, a magnetic parameter, a Brownian motion parameter, a thermophoresis parameter, and a Lewis number, respectively.

The engineering concerns of the present study are the skin friction coefficient C_f, the local Nusselt number Nu_x and the local Sherwood number Sh_x, defined respectively as:

$$C_f = \frac{\tau_w}{\rho u_w^2}, \qquad \mathrm{Nu}_x = \frac{x q_w}{k(T_f - T_\infty)}, \qquad \mathrm{Sh}_x = \frac{x h_m}{D_B(C_w - C_\infty)}, \tag{2.14}$$

where the wall shear stress τ_w, wall heat flux q_w and wall mass flux h_m are given by

$$\tau_w = \mu \left(\frac{\partial u}{\partial y}\right)_{y=0}, \quad q_w = -k \left(\frac{\partial T}{\partial y}\right)_{y=0}, \quad h_m = -D_B \left(\frac{\partial C}{\partial y}\right)_{y=0}. \tag{2.15}$$

By using the above equations,

$$C_f \sqrt{\mathrm{Re}_x} = -f''(0), \qquad \frac{\mathrm{Nu}_x}{\sqrt{\mathrm{Re}_x}} = -\theta'(0), \qquad \frac{\mathrm{Sh}_x}{\sqrt{\mathrm{Re}_x}} = -\phi'(0) \tag{2.16}$$

are obtained, where Re_x, Nu_x, Sh_x are local Reynolds number, local Nusselt number and local Sherwood number, respectively.

3. Numerical solution

The system of three coupled ordinary differential Eqs (2.9)–(2.11) subjected to the boundary conditions Eq. (2.12) is inspected numerically using SQLM for different values of main parameters viz. slip parameters γ and δ, the Prandtl number Pr, the magnetic parameter M, the Brownian motion parameter N_b, the thermophoresis parameter N_t and the Lewis number Le.

The main idea behind this method is identifying univariate and multivariate nonlinear terms of function and its derivative in each of the equations of the system (2.9)–(2.11), making the terms linear and applying the Chebychev pseudo-spectral collocation method (see [5]).

By applying the spectral quasilinearization method, Eqs (2.9)–(2.11) give the following iterative sequence of linear differential equations:

$$f'''_{r+1} + a_{1,r} f''_{r+1} + a_{2,r} f'_{r+1} + a_{3,r} f_{r+1} = a_{4,r}, \tag{3.1}$$

$$\theta''_{r+1} + b_{1,r} \theta'_{r+1} + b_{2,r} f'_{r+1} + b_{3,r} \phi'_{r+1} = b_{4,r}, \tag{3.2}$$

$$\phi''_{r+1} + c_{1,r}\phi'_{r+1} + c_{2,r}f_{r+1} + c_{3,r}\theta'_{r+1} = c_{4,r}, \tag{3.3}$$

where the terms containing $r+1$ subscripts denote current approximations and the terms containing r subscripts denote previous approximations. The corresponding boundary conditions are:

$$\begin{aligned} &f_{r+1}(0) = 0, \qquad f'_{r+1}(0) = 1 + \gamma f''_{r+1}(0) + \delta f'''_{r+1}(0), \qquad f'_{r+1}(\infty) \to 1, \\ &\theta'_{r+1}(0) = -B_i(1 - \theta_{r+1}(0)), \quad \phi_{r+1}(0) = 1, \quad \theta_{r+1}(\infty) = \phi_{r+1}(\infty) \to 0, \end{aligned} \tag{3.4}$$

where

$$a_{1,r} = f_r, \qquad a_{2,r} = -2\beta f'_r - M, \qquad a_{3,r} = f''_r, \qquad a_{4,r} = f_r f''_r - f'^2_r),$$

$$b_{1,r} = \Pr(f_r + N_b\phi'_r + 2N_t\theta'_r), \qquad b_{2,r} = \Pr\theta_r, \qquad b_{3,r} = \Pr N_b\theta'_r,$$

$$b_{4,r} = \Pr f_r(\theta'_r) + \Pr N_b\theta'_r(\phi'_r) + \Pr N_t(\theta'_r)^2,$$

$$c_{1,r} = \Pr \operatorname{Le} f_r, \quad c_{2,r} = \operatorname{Le} \Pr \phi'_r, \quad c_{3,r} = 0, \quad c_{4,r} = \operatorname{Le} \Pr f_r(\phi'_r) - \left(\frac{N_t}{N_b}\right)\theta''_r.$$

The physical domain on which the system of governing Eqs (2.9)–(2.11) defined in $[0,\infty)$ is moved to $[-1,1]$ using the transformation $x = \frac{2\eta}{L_\infty} - 1$, where L_∞ is a scaling parameter assumed to be large and the interval $[0,\infty)$ is replaced by $[0, L_\infty]$. The spectral collocation method is applied to the system of Eqs (3.1)–(3.3), and the differentiation matrix $\mathbf{D} = \frac{2D}{L_\infty}$ is used to approximate the derivatives of unknown variables, where $\mathbf{D}$ is $(N+1)\times(N+1)$ Chebyshev differentiation matrix (see [1]). The system of Eqs (3.1)–(3.3) is solved as a coupled matrix:

$$\begin{bmatrix} \Lambda_{11} & \Lambda_{12} & \Lambda_{13} \\ \Lambda_{21} & \Lambda_{22} & \Lambda_{23} \\ \Lambda_{31} & \Lambda_{32} & \Lambda_{33} \end{bmatrix} \begin{bmatrix} F_{r+1} \\ \Theta_{r+1} \\ \Phi_{r+1} \end{bmatrix} = \begin{bmatrix} R_1 \\ R_2 \\ R_3 \end{bmatrix} \tag{3.5}$$

with transformed boundary condition

$$\begin{gathered} F_{r+1}(x_{N_x}) = 0, \qquad F_{r+1}(x_{N_{x-1}}) = 1 + \gamma F'_{r+1}(x_{N_x}) + \delta F''_{r+1}(x_{N_x}), \\ F_{r+1}(x_0) = 1, \\ \Theta'_{r+1}(x_{N_x}) = -B_i(1 - \Theta_r(x_{N_x})), \qquad \Theta_{r+1}(x_0) = 0, \\ \Phi_{r+1}(x_{N_x}) = 1, \qquad \Phi_{r+1}(x_0) = 0, \end{gathered} \tag{3.6}$$

where

$$R_1 = a_{4,r}, \qquad R_2 = b_{4,r}, \qquad R_3 = c_{4,r},$$

$$\Lambda_{11} = \mathbf{D}^3 + \mathrm{diag}(a_{1,r})\mathbf{D}^2 - \mathrm{diag}(a_{2,r})\mathbf{D} + \mathrm{diag}(a_{3,r}), \qquad \Lambda_{12} = \mathbf{0}; \qquad \Lambda_{13} = \mathbf{0},$$

$$\Lambda_{21} = \mathrm{diag}(b_{2,r}), \qquad \Lambda_{22} = \mathbf{D}^2 + \mathrm{diag}(b_{1,r})\mathbf{D}, \qquad \Lambda_{23} = \mathrm{diag}(b_{3,r})\mathbf{D},$$

$$\Lambda_{31} = \mathrm{diag}(c_{2,r}), \qquad \Lambda_{32} = \mathrm{diag}(c_{3,r})\mathbf{D}, \qquad \Lambda_{33} = \mathbf{D}^2 + \mathrm{diag}(c_{1,r})\mathbf{D},$$

$$F_{r+1} = [f_{r+1,0}, f_{r+1,1}, ..., f_{r+1,N}]^{\mathrm{T}},$$

$$\Theta_{r+1} = [\theta_{r+1,0}, \theta_{r+1,1}, ..., \theta_{r+1,N}]^{\mathrm{T}},$$

$$\Phi_{r+1} = [\phi_{r+1,0}, \phi_{r+1,1}, ..., \phi_{r+1,N},]^{\mathrm{T}},$$

are vectors of sizes $(N_x+1)\times 1$, diag(...) represents a diagonal matrix of vectors, and $\mathbf{0}$ is a zero vectors of size $(N_x+1)\times(N_x+1)$.

The suitable initial approximations that satisfy the governing boundary conditions of the boundary layer Eqs (2.9)–(2.11) are

$$f_0(\eta) = \frac{1-e^{-\eta}}{1+\gamma-\delta}, \qquad \theta_0(\eta) = \frac{B_i}{1+B_i}e^{-\eta}, \qquad \phi_0(\eta) = e^{-\eta}. \tag{3.7}$$

4. Results and discussion

The coupled transmuted equations from momentum, energy and concentration Eqs (2.9)–(2.11) with the boundary conditions Eq. (2.12) were numerically computed using the spectral quasilinearization method. The outcomes obtained are shown in figures and tables.

Figuers 2 and 3 depict the non-dimensional velocity component f for various values of the first-order slip parameter γ and the second-order slip parameter δ. These figures specify that the boundary stratum width reduced with the rising values of γ while it the increased with increasing values of δ. These results are found to be in an excellent agreement with the report of [11].

The velocity graph $f'(\eta)$ for different values of the first-order slip parameter γ and second-order slip parameter δ is depicted in Figs 4 and 5. These figures illustrate that $f'(\eta)$ is decreasing with increasing the values of γ and δ. Moreover, the velocity boundary thickness is diminishing as the values of γ and δ are increasing in absolute value, and also the velocity at the surface decreases as the values of γ and δ increase.

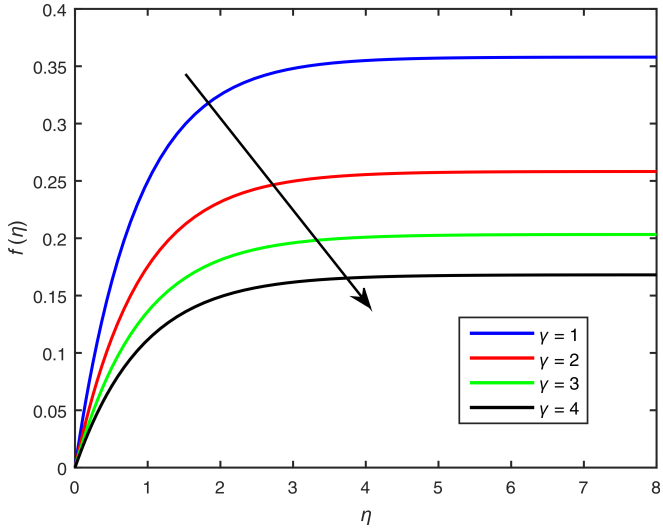

FIG. 2. Graph of f profile for different values of γ when $N_b = N_t = 0.5$, $\mathrm{Pr} = 1$, $\mathrm{Le} = 5$, $M = 1$, $\delta = -0.1$.

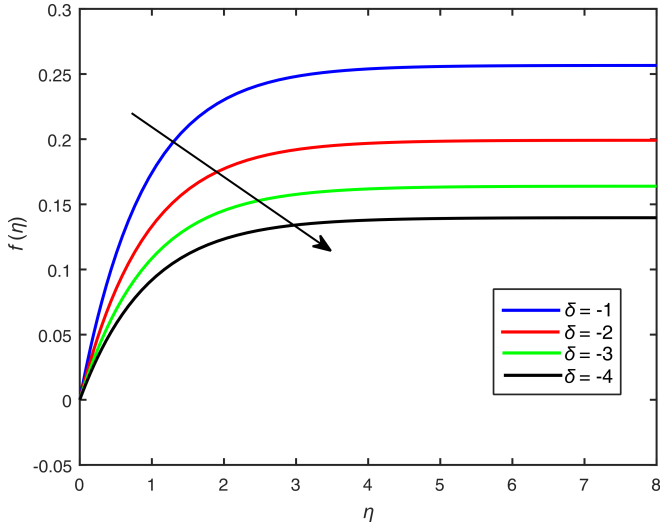

FIG. 3. Graph of f profile for different values of δ when $N_b = N_t = 0.5$, $\mathrm{Pr} = 1$, $\mathrm{Le} = 5$, $M = \gamma = 1$.

Figure 6 shows the effect of the first-order slip parameter γ and second-order δ on the graph skin friction profile $f''(\eta)$. It can be seen that the graphs are an increasing function of both parameters in absolute value. Moreover, the coefficient of skin friction is an increasing function of both parameters.

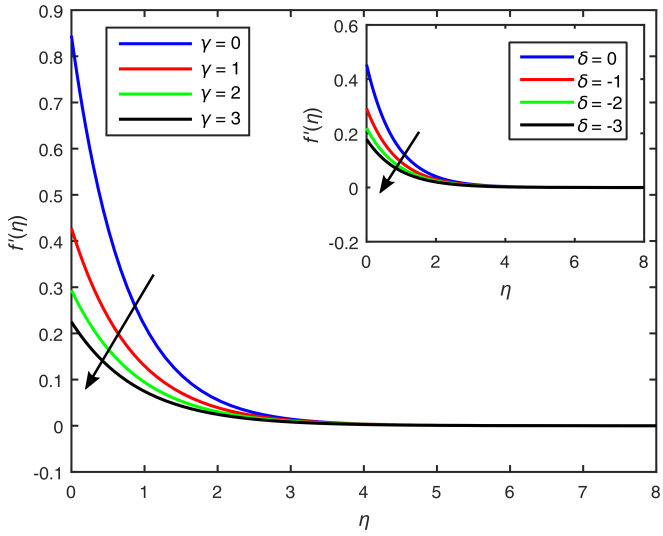

FIG. 4. Velocity profile for different values of γ and δ when $N_b = N_t = 0.5$, $\mathrm{Pr} = 1$, $\mathrm{Le} = 5$, $M = 1$.

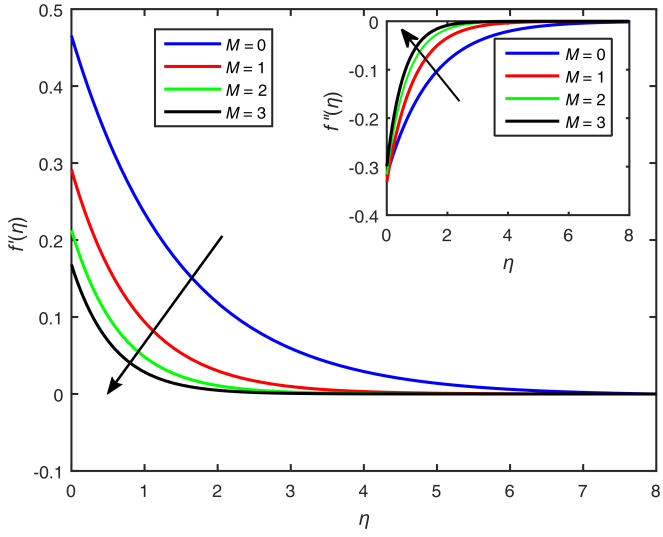

FIG. 5. Velocity profile graph and f'' graph for different values of M when $N_b = N_t = 0.5$, $\delta = -1$, $\mathrm{Le} = 5$, $\mathrm{Pr} = \gamma = 1$.

The effects of slip parameters γ and δ, convective parameter B_i, thermophoresis parameter N_t and Brownian motion parameter N_b on temperature profile are given in Figs 7–9. In Fig. 7, it can be observed that the temperature of the flow field is a decreasing function of both slip parameters. However, its thermal boundary thickness is an increasing function of both parameters.

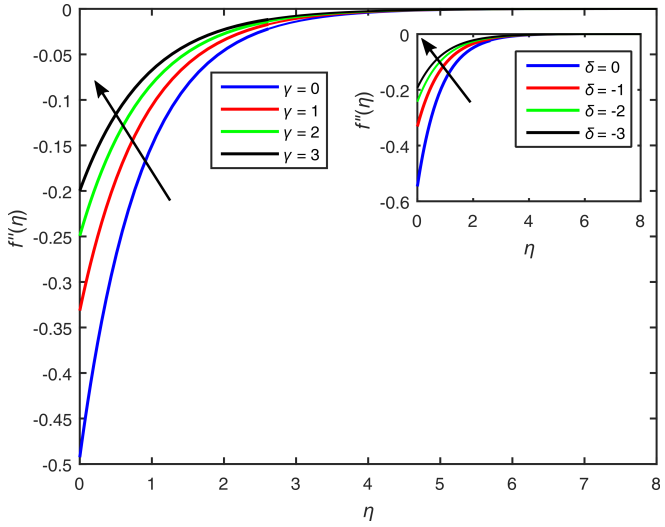

FIG. 6. $f''(\eta)$ profile for different values of γ and δ when $N_b = N_t = 0.5$, $\mathrm{Pr} = 1$, $\mathrm{Le} = 5$, $M = 1$.

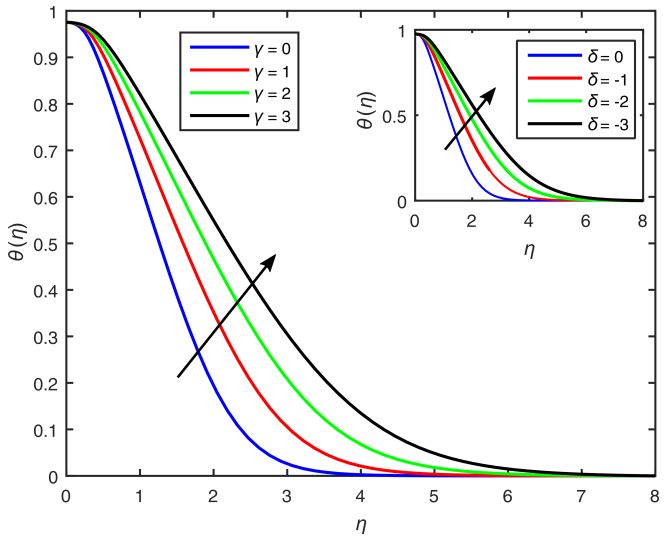

FIG. 7. Temperature profile for different values of γ and δ when $N_t = N_b = 0.5$, $\mathrm{Pr} = 7$, $\mathrm{Le} = 10$, $M = 1$, $B_i = 5$.

Figure 8 sketches the impact of convective heating on temperature graph. Convective heating enhances the heat holding capacity of the fluid as a result of the thermal boundary layer thickness being boosted. Figure 9 shows the influence of the change of Brownian motion parameter N_b and thermophoresis parameter

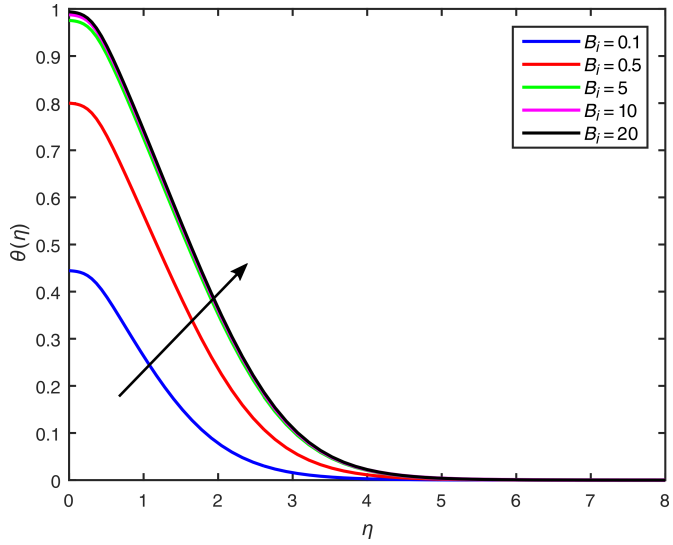

FIG. 8. Temperature profile for different values of convective parameter B_i when $N_t = N_b = 0.5$, $\gamma = M = 1$, $\mathrm{Pr} = 7$, $\mathrm{Le} = 10$.

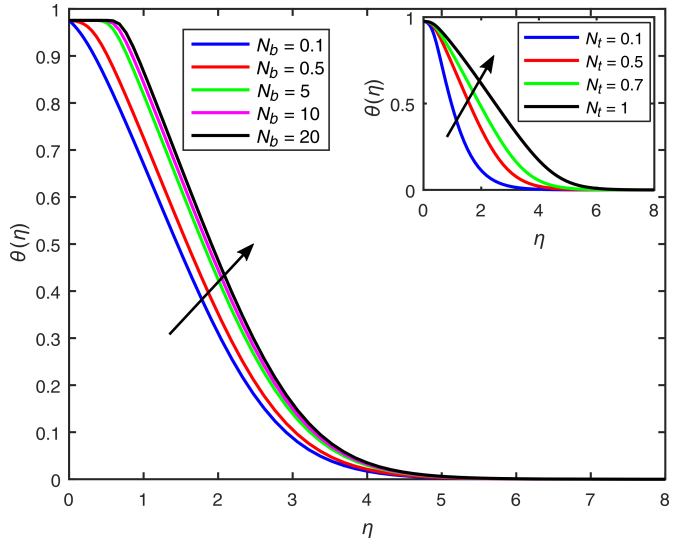

FIG. 9. Temperature graph for different values of N_b and N_t when $\mathrm{Pr} = 7$, $\gamma = M = 1$, $\mathrm{Le} = 10$, $\delta = -1$, $B_i = 5$.

N_t on the temperature profile graph. As the values of N_t and N_b increase, the temperature of the flow field increases, moreover, the thermal boundary layer thickness grows.

The concentration profile graphs for both slip parameters are displayed in Fig. 10. As observed in the cases of temperature graph, the concentration graph is an increasing function of both parameters; also, the concentration boundary layer thickness is enlarged when both parameters γ and δ are increased. Figure 11

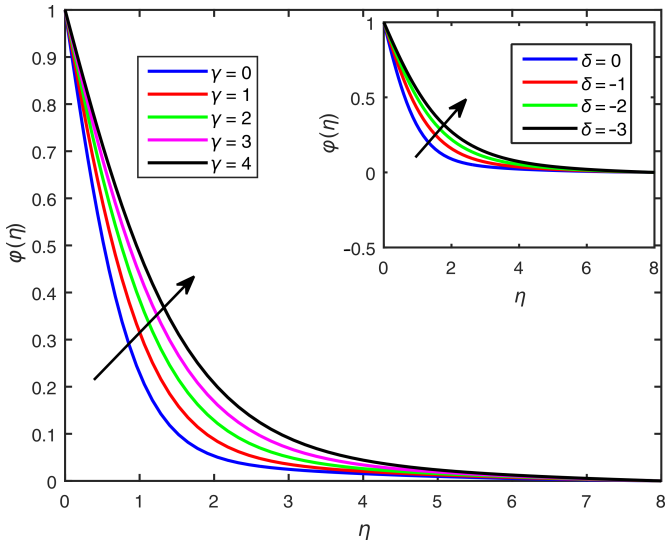

FIG. 10. Concentration profile for different values of γ and δ when $Nt = 0.2$, $Nb = 0.5$, $\mathrm{Pr} = M = 1$, $B_i = \mathrm{Le} = 5$.

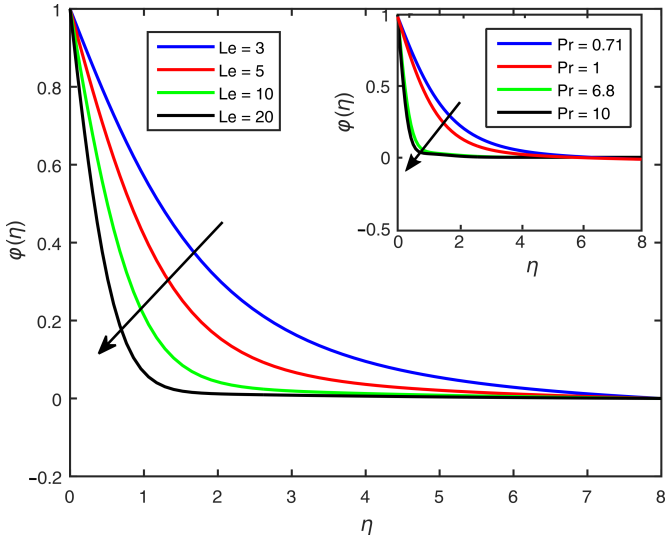

FIG. 11. Concentration graph for different values of Le and Pr when $N_t = N_b = 0.5$, $\gamma = M = 1$, $\delta = -1$, $B_i = 5$.

illustrates the concentration graph with the impact of changing the Prandtl number Pr and Lewis number Le. As usual, both parameters are against the development of the graphs.

The influence of the first-order slip parameter γ and the second-order slip parameter δ along with the magnetic field parameter M on the graph of the local skin friction coefficient is displayed in Figs 12 and 13. The graphs show that

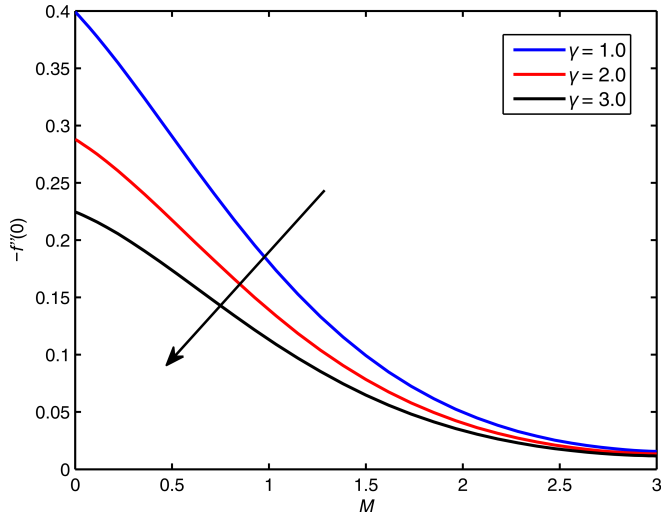

FIG. 12. Graph of skin friction coefficient for different values of γ when magnetic field parameter M varies.

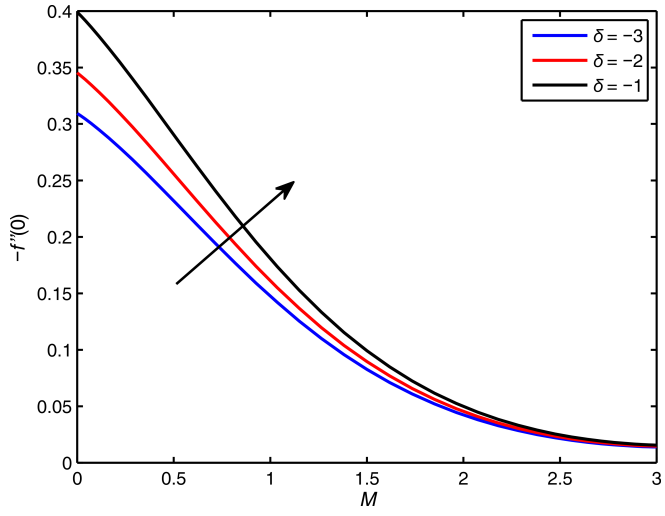

FIG. 13. Graph of skin friction coefficient for different values of δ when magnetic field parameter M varies.

both parameters diminish the skin friction coefficient $f''(0)$. Figure 14 shows the impact of the convective parameter B_i along N_t for the local Nusselt number. Both parameters favor the development of the local Nusselt number $\theta'(0)$.

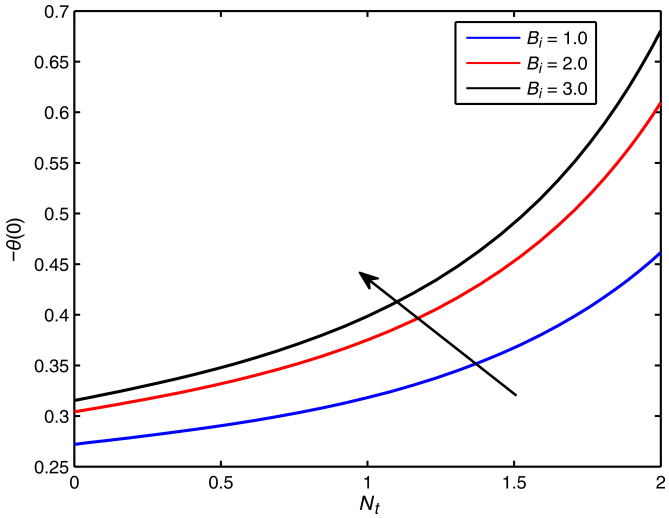

FIG. 14. Graph of local Nusselt number $\theta'(0)$ for different values of B_i when magnetic field parameter N_t varies.

In order to assess the accuracy of the numerical algorithm used, comparison with earlier existing researches has been made. From Table 1, it can be observed that the values of the skin friction coefficient $f''(0)$ computed in this paper for varied values of γ, when $M = \delta = 0$, are in an excellent agreement with the

Table 1. Comparison of values of $f''(0)$ with slip factor γ when $M = \delta = 0$.

γ	Present result (SQLM)	Present result (bvp4c)	[21]	[22]
0.0	1.00000002	1.00000002	1.000000	1.001154
0.1	0.87208251	0.87208251	0.872082	0.871447
0.2	0.77637712	0.77637712	0.776377	0.774933
0.3	0.70154827	0.70154827	0.701548	0.699738
0.5	0.59119558	0.59119558	0.591196	0.589195
1.0	0.43015992	0.43015992	0.430160	0.428450
2.0	0.28398008	0.28398008	0.283980	0.282893
3.0	0.21405559	0.21405559	0.214055	0.213314
5.0	0.14484142	0.14484142	0.144841	0.144430
10.0	0.08124399	0.08124399	0.081243	0.081091
20.0	0.04379099	0.04379099	0.043790	0.043748

results reported by [21] and [22]. To further authenticate the method used in this paper, the author checked the solution with another method called bvp4c, and confirmed that the method used is appropriate for finding the solution of the problem.

Comparison of local Nusselt number $\theta'(0)$ and local Sherwood number $\phi'(0)$ for different values of Brownian motion parameter N_b and thermophoresis parameter N_t by ignoring the impact of M, γ and δ parameters when the values of $B_i \to \infty$ with bvp4c method has been shown in Table 2, and both methods show outstanding agreement with each other. Comparison of the results of this study with the literature reports and with the bvp4c method is shown in Tables 1 and 2. It indicates a first-rate agreement and therefore highly accurate results of this research.

Table 2. Computation of local Nusselt number $\theta'(0)$ and Sherwood number $\phi'(0)$ at Le = 10, Pr = 10, $\gamma = \delta = M = 0$, $B_i \to \infty$ for different values of N_b and N_t with SQLM and bvp4c methods.

N_b	N_t	SQLM method		bvp4c method	
		$\theta'(0)$	$\phi'(0)$	$\theta'(0)$	$\phi'(0)$
0.1	0.1	0.63698391	8.13797515	0.63698391	8.13797515
0.2		0.25925991	8.04781286	0.25925990	8.04781286
0.3		0.10246429	7.96747625	0.10246429	7.96747625
0.4		0.03974764	7.91412275	0.03974767	7.91412274
0.5		0.01523411	7.87932302	0.01523417	7.87932301
0.1	0.1	0.63698391	8.13797515	0.63698391	8.13797515
	0.2	0.43866320	8.48336868	0.43866320	8.48336868
	0.3	0.32116931	8.73407764	0.32116931	8.73407764
	0.4	0.24780514	8.90353248	0.24780514	8.90353248
	0.5	0.19950871	9.01765972	0.19950871	9.01765972

5. Conclusions

This article presented the impact of the second-order slip flow and convective heating on MHD boundary layer flow and heat transfer of a nanofluid over a stretching surface. The boundary layer equations governing the flow problem were transformed to a couple of high-order non-linear ordinary differential equations using the similarity transformation. The obtained differential equations were solved numerically using both spectral quasilinearization method and bvp4c from Matlab software, and the solutions obtained with both methods are in excellent conformity. The concise outcomes of the study are:

1) The magnetic field has a similar effect on the velocity graph and skin friction graph.
2) Both slip parameters have a reducing effect on the velocity graph.
3) Brownian motion parameter N_b and thermophoresis parameter N_t favoured the temperature graph.
4) Prandtl number and Lewis number have similar effect on concentration graph.

References

1. Trefethen L.N., Spectral methods in MATLAB, *Siam*, Philadelphia, 2000.
2. Shateyi S., Makinde O.D., Hydromagnetic stagnation-point flow towards a radially stretching convectively heated disk, *Mathematical Problems in Engineering*, **2013**, Article ID 616947, 8 pages, 2013.
3. Majeed A., Javed T., Shami S., Numerical analysis of Walters-B fluid flow and heat transfer over a stretching cylinder, *Canadian Journal of Physics*, **94**(5): 522–530, 2016.
4. Motsa S.S., Dlamini P.G., Khumalo M., Spectral relaxation method and spectral quasilinearization method for solving unsteady boundary layer flow problems, *Advances in Mathematical Physics*, **2014**, Article ID 341964, 12 pages, 2014.
5. Motsa S.S., Makukula Z.G, Shateyi S., Spectral local linearisation approach for natural convection boundary layer flow, *Mathematical Problems in Engineering*, **2013**, Article ID 765013, 7 pages, 2013.
6. Magagula V.M., Motsa S.S., Sibanda P., Dlamini P.G., On a bivariate spectral relaxation method for unsteady magneto-hydrodynamic flow in porous media, *SpringerPlus*, **5**(1): Article number 455, 2016.
7. Motsa S., A new spectral relaxation method for similarity variable nonlinear boundary layer flow systems, *Chemical Engineering Communications*, **201**(2): 241–256, 2014.
8. Ibrahim W., Tulu A., Magnetohydrodynamic (MHD) boundary layer flow past a wedge with heat transfer and viscous effects of nanofluid embedded in porous media, *Mathematical Problems in Engineering*, **2019**, Article ID 4507852, 12 pages, 2019.
9. Fang T., Yao S., Zhang J., Aziz A., Viscous flow over a shrinking sheet with a second order slip flow model, *Communications in Nonlinear Science and Numerical Simulation*, **15**(7): 1831–1842, 2010.
10. Fang T., Aziz A., Viscous flow with second-order slip velocity over a stretching sheet, *Zeitschrift für Naturforschung A.*, **65**(12): 1087–1092, 2010.
11. Nandeppanavar M.M., Vajravelu K., Abel M.S., Siddalingappa M., Second order slip flow and heat transfer over a stretching sheet with non-linear Navier boundary condition, *International Journal of Thermal Sciences*, **58**: 143–150, 2012.
12. Roşca A.V., Pop I., Flow and heat transfer over a vertical permeable stretching/shrinking sheet with a second order slip, *International Journal of Heat and Mass Transfer*, **60**: 355–364, 2013.

13. Roşca N.C., Pop I., Mixed convection stagnation point flow past a vertical flat plate with a second order slip: heat flux case, *International Journal of Heat and Mass Transfer*, **65**: 102–109, 2013.

14. Turkyilmazoglu M., Heat and mass transfer of MHD second order slip flow, *Computers & Fluids*, **71**: 426–434, 2013.

15. Singh G., Chamkha A.J., Dual solutions for second-order slip flow and heat transfer on a vertical permeable shrinking sheet, *Ain Shams Engineering Journal*, **4**(4): 911–917, 2013.

16. Broutman D., A practical guide to pseudospectral methods, by B. Fornberg, Cambridge University Press, 1996; *Journal of Fluid Mechanics*, **360**: 375–378, 1998.

17. Gottlieb D., Orszag S.A., Numerical analysis of spectral methods: theory and applications, *Society for Industrial and Applied Mathematics*, Philadelphia, 1983.

18. Canuto C., Hussaini M.Y., Quarteroni A., Zang T.A., Spectral methods in fluid dynamics, *Springer-Verlag*, New York 1988.

19. Khan W.A., Pop I., Boundary-layer flow of a nanofluid past a stretching sheet, *International Journal of Heat and Mass Transfer*, **53**(11–12): 2477–2483, 2010.

20. Wu L., A slip model for rarefied gas flows at arbitrary Knudsen number, *Applied Physics Letters*, **93**(25): 253103, 2008.

21. Noghrehabadi A., Pourrajab R., Ghalambaz M., Effect of partial slip boundary condition on the flow and heat transfer of nanofluids past stretching sheet prescribed constant wall temperature, *International Journal of Thermal Sciences*, **54**: 253–261, 2012.

22. Sahoo B., Effects of partial slip, viscous dissipation and Joule heating on Von Kármán flow and heat transfer of an electrically conducting non-Newtonian fluid, *Communications in Nonlinear Science and Numerical Simulation*, **14**(7): 2982–2998, 2009.

Received May 31, 2019; accepted version September 30, 2019.
